Parquet approximation for the 4×4 Hubbard cluster

S. X. Yang,[1] H. Fotso,[1] J. Liu,[1] T. A. Maier,[2,3] K. Tomko,[4] E. F. D'Azevedo,[2] R. T. Scalettar,[5] T. Pruschke,[6] and M. Jarrell[1]
[1]*Department of Physics and Astronomy, Louisiana State University, Baton Rouge, Louisiana 70803, USA*
[2]*Computer Science and Mathematics Division, Oak Ridge National Laboratory, Oak Ridge, Tennessee 37831, USA*
[3]*Center for Nanophase Materials Sciences, Oak Ridge National Laboratory, Oak Ridge, Tennessee 37831, USA*
[4]*Ohio Supercomputer Center, Columbus, Ohio 43212, USA*
[5]*Physics Department, University of California, Davis, California 95616, USA*
[6]*Department of Physics, University of Göttingen, 37077 Göttingen, Germany*
(Received 24 June 2009; published 21 October 2009)

We present a numerical solution of the parquet approximation, a conserving diagrammatic approach which is self-consistent at both the single-particle and the two-particle levels. The fully irreducible vertex is approximated by the bare interaction thus producing the simplest approximation that one can perform with the set of equations involved in the formalism. The method is applied to the Hubbard model on a half-filled 4×4 cluster. Results are compared to those obtained from determinant quantum Monte Carlo (DQMC), FLuctuation EXchange (FLEX), and self-consistent second-order approximation methods. This comparison shows a satisfactory agreement with DQMC and a significant improvement over the FLEX or the self-consistent second-order approximation.

DOI: 10.1103/PhysRevE.80.046706 PACS number(s): 02.60.−x, 71.10.−w, 71.27.+a

I. INTRODUCTION

Over the past 50 years, many different techniques have been devised and employed to study strongly correlated electron systems. Unfortunately, advantages of the successful attempts were usually outweighed by their limitations. Recently, because of the progress in computer technology, complex diagrammatic approaches have received increased attention. Although Baym and Kadanoff's Φ derivability [1,2] does not guarantee the physical validity of a theory, their framework enables the generation of conserving approximations which are guaranteed to satisfy a variety of Ward identities. For these reasons, the FLuctuation EXchange (FLEX) approximation [3,4] has been intensively studied over the years. Its major disadvantage however is that it represents a conserving approximation at the single-particle level only. Thus, the physical validity of the approximation appears to be questionable as the vertices are either overestimated or underestimated and the Pauli exclusion principle is not respected properly [5]. In contrast, the parquet formalism [6] introduced by de Dominicis *et al.* in 1964 is a conserving approximation which is self-consistent also at the two-particle level and one may hope that it resolves at least some of the limitations FLEX has. Unfortunately, it has extremely complicated structure and was, apart from applications to the Anderson impurity model and the one-dimensional (1D) Hubbard model with small system size [7,8], hitherto also computationally out of reach. To circumvent this limitation, Bickers *et al.* introduced the so-called pseudoparquet approximation [3] which attempts to improve on the FLEX without introducing the complexity of the full Parquet equations. But this approach fails to properly address the full frequency and momentum dependence of the scattering processes. Only very recently, due to the great advance of the parallel computing and the tremendous increase in computer memory, has it become possible to fully solve this approximation for the first time.

The paper is organized as follows. In part I we present the formalism and the resulting equations. In part II, we discuss the algorithm and the numerical difficulties that arising. In part III, we present first results obtained from the parquet approximation (PA) for the two-dimensional Hubbard model and their comparison to other conserving approximation methods such as FLEX and self-consistent second-order approximation (SC2nd). As a benchmark, we compare these results against the determinant quantum Monte Carlo (DQMC) which provides a numerically exact result.

II. FORMALISM

A. Vertex functions

Standard perturbative expansions attempt to describe all the scattering processes as single- or two-particle Feynman diagrams. In the single-particle formalism the self-energy describes the many-body processes that renormalize the motion of a particle in the interacting background of all the other particles. In the two-particle context, with the aid of the parquet formalism, one is able to probe the interactions between particles in greater detail using the so-called vertex functions, which are matrices describing the two particle scattering processes. For example, the reducible two-particle vertex $F_h^{ph}(12;34)$ describes the amplitude of a particle-hole pair scattered from its initial state $|3,4\rangle$ into the final state $|1,2\rangle$. Here, $i=1,2,3,4$ represents a set of indices which combines the momentum $\mathbf{k}_i$, the matsubara frequency $i\omega_{n_i}$ and, if needed, the spin σ_i and band index m_i.

In general, depending on how particles or holes are involved in the scattering processes, one can define three different two-particle scattering channels. These are the particle-hole (p-h) horizontal channel, the p-h vertical channel and the particle-particle (p-p) channel. For the Hubbard model, the spin degree of freedom further divides the particle-particle channel into triplet and singlet channels

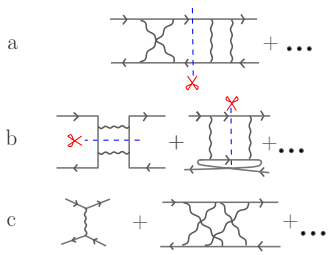

FIG. 1. (Color online) Different classes of diagrams; the solid line represents the single-particle Green's function and the wavy line represents the Coulomb interaction: here we use the p-h horizontal channel for illustration. (a) Reducible diagrams: can be separated into two parts by cutting two horizontal Green's function lines. (b) Irreducible diagrams: can only be separated into two parts by cutting two Green's function lines in the other two channels. (c) Fully irreducible diagrams: cannot be split in two parts by breaking two Green's function lines in any channel.

while the particle-hole is divided into density and magnetic channels.

One can further discriminate the vertices according to their topology. Starting from the reducible vertex F introduced above, we may define the irreducible vertex Γ corresponding to the subclass of diagrams in F that cannot be separated into two parts by cutting two horizontal Green's function lines. Similarly, the fully irreducible vertex Λ corresponds to the subclass of diagrams in Γ that cannot be split into two parts by cutting two Green's function lines in any channel. An illustration of these different types of vertices is provided in Fig. 1.

The Pauli exclusion principle produces the so-called crossing symmetries which in turn yield relationships between these vertices in the different channels. This enables us to reduce the independent channels defined for the theory to the particle-particle and the particle-hole horizontal channels.

B. Equations

The parquet formalism assumes the complete knowledge of the fully irreducible vertices and provides a set of equations which are self-consistent at both the single- and two-particle levels. The connection between the single- and two-particle quantities is through the Schwinger-Dyson equation which connects the reducible vertex F to the self-energy Σ. It is an exact equation derived from the equation of motion and has the following form:

$$\Sigma(P) = -\frac{UT^2}{4N}\sum_{P',Q}\{G(P')G(P'+Q)G(P-Q)[F_d(Q)_{P-Q,P'} - F_m(Q)_{P-Q,P'}] + G(-P')G(P'+Q)G(-P+Q) \times [F_s(Q)_{P-Q,P'} + F_t(Q)_{P-Q,P'}]\} \quad (1)$$

where G is the single-particle Green's function, which itself can be calculated from the self-energy using the Dyson's equation,

$$G^{-1}(P) = G_0^{-1}(P) - \Sigma(P). \quad (2)$$

Here, the indices P, P', and Q combine momentum $\mathbf{k}$ and Matsubara frequency $i\omega_n$, i.e., $P=(\mathbf{k}, i\omega_n)$.

The reducible and the irreducible vertices in a given channel are related by the Bethe-Salpeter equation. It has the following form:

$$F_r(Q)_{P,P'} = \Gamma_r(Q)_{P,P'} + \Phi_r(Q)_{P,P'} \quad (3)$$

$$F_{r'}(Q)_{P,P'} = \Gamma_{r'}(Q)_{P,P'} + \Psi_{r'}(Q)_{P,P'} \quad (4)$$

where $r=d$ or m for the density and magnetic channels respectively and $r'=s$ or t for the singlet and triplet channels, and we are using the vertex ladders which are defined as

$$\Phi_r(Q)_{P,P'} \equiv \sum_{P''} F_r(Q)_{P,P''}\chi_0^{ph}(Q)_{P''}\Gamma_r(Q)_{P'',P'}, \quad (5)$$

$$\Psi_{r'}(Q)_{P,P'} \equiv \sum_{P''} F_{r'}(Q)_{P,P''}\chi_0^{pp}(Q)_{P''}\Gamma_{r'}(Q)_{P'',P'}, \quad (6)$$

χ_0 is the direct product of two single-particle Green's functions and is defined according to the particle-particle or the particle-hole channel.

In a similar manner, the irreducible vertex and the fully irreducible vertex are related by the parquet equation. This set of equations expresses the fact that the irreducible vertex in a given channel is still reducible in the other two channels. The parquet equation has the following form in the different channels:

$$\Gamma_d(Q)_{PP'} = \Lambda_d(Q)_{PP'} - \frac{1}{2}\Phi_d(P'-P)_{P,P+Q} - \frac{3}{2}\Phi_m(P'-P)_{P,P+Q} + \frac{1}{2}\Psi_s(P+P'+Q)_{-P-Q,-P} + \frac{3}{2}\Psi_t(P+P'+Q)_{-P-Q,-P}, \quad (7)$$

$$\Gamma_m(Q)_{PP'} = \Lambda_m(Q)_{PP'} - \frac{1}{2}\Phi_d(P'-P)_{P,P+Q} + \frac{1}{2}\Phi_m(P'-P)_{P,P+Q} - \frac{1}{2}\Psi_s(P+P'+Q)_{-P-Q,-P} + \frac{1}{2}\Psi_t(P+P'+Q)_{-P-Q,-P}, \quad (8)$$

$$\Gamma_s(Q)_{PP'} = \Lambda_s(Q)_{PP'} + \frac{1}{2}\Phi_d(P'-P)_{-P',P+Q} - \frac{3}{2}\Phi_m(P'-P)_{-P',P+Q} + \frac{1}{2}\Phi_d(P+P'+Q)_{-P',-P} - \frac{3}{2}\Phi_m(P+P'+Q)_{-P',-P}, \quad (9)$$

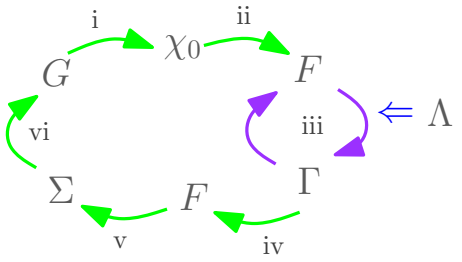

FIG. 2. (Color online) Schematic illustration for the different steps in solving the parquet approximation equations self-consistently.

$$\Gamma_t(Q)_{PP'} = \Lambda_t(Q)_{PP'} + \frac{1}{2}\Phi_d(P'-P)_{-P',P+Q} + \frac{1}{2}\Phi_m(P'-P)_{-P',P+Q} - \frac{1}{2}\Phi_d(P+P'+Q)_{-P',-P} - \frac{1}{2}\Phi_m(P+P'+Q)_{-P',-P}. \quad (10)$$

The Bethe-Salpeter and parquet equations are also exact and derived from the categorization of the Feynman diagrams.

The above discussion of the structure of the parquet formalism is far from being exhaustive and is merely intended to make the paper reasonably self-contained. For a more detailed description of the parquet formalism, we refer the reader to Bickers *et al.* [7,9]. Our actual goal is to numerically solve these equations self-consistently for the Hubbard model on a two dimensional cluster. The algorithm for this solution is described in the next section.

III. ALGORITHM AND COMPUTATIONAL CHALLENGE

The set of equations discussed above are solved self-consistently as illustrated in the self-consistency loop in Fig. 2. One starts with a guess of the single-particle Green's function or self-energy. This can, for example, be taken from the second-order approximation. The reducible and the irreducible vertices are also initialized with the bare interaction. The self-consistency loop can then be described as follows:

(i) first we calculate the bare susceptibility χ_0 which is given by the product of two Green's functions.

(ii) Next this bare susceptibility is used to calculate F through the Bethe-Salpeter equation.

(iii) We then proceed with updating the irreducible vertices Γ by solving the parquet equation.

This step requires the input of the fully irreducible vertex Λ. In the context of the parquet approximation which we study here it is taken to be the bare interaction. It however can also be extracted from some more sophisticated methods.

(iv) It is followed by a calculation of the new F through the Bethe-Salpeter equation.

(v) This value of F is then used to update the self-energy through the Schwinger-Dyson equation.

(vi) The Dyson's equation is solved for the Green's function G.

This loop is repeated until convergence of the self-energy Σ is achieved within a reasonable criterion.

Unfortunately, this loop becomes unstable when the strength of the Coulomb interaction is increased or the temperature is lowered. As we believe that this instability is purely numerical in origin and related to the iterative nature of the algorithm, we have to extend the above scheme to account for this problem. For example, one possibility is to start with an overestimated self-energy and to damp it along with the irreducible vertex between two iterations according to

$$\Sigma = \alpha_1 \Sigma_{new} + (1-\alpha_1)\Sigma_{old}, \quad (11)$$

$$\Gamma = \alpha_2 \Gamma_{new} + (1-\alpha_2)\Gamma_{old}, \quad (12)$$

where α_1 and α_2 are some damping parameters.

Another possibility is to rewrite the coupled Bethe-Salpeter and parquet equations in the form $f(\mathbf{x})=0$ and apply a variant of a Newton's root searching method. Then we can take advantage of the existing linear solvers such as BiCGS [10], GMRES [11] or the Broyden algorithm [12].

One major advantage that the parquet formalism has over exact diagonalization (ED) or quantum Monte Carlo (QMC) is that it scales algebraically with the volume of the system in space time for any choice of parameters including those that lead to a sign problem in QMC. The most time-consuming part of the formalism is the solution of the Bethe-Salpeter and the parquet equations, where the computational time scales as $O(n_t^4)$ where $n_t = n_c \times n_f$, n_c being the number of sites on the cluster and n_f the number of Matsubara frequencies. Although the scaling is better than that of ED or QMC when the sign problem is severe, one can see that the complexity quickly grows beyond the capacity of usual desktop computers with increasing system size, and large-scale supercomputer systems have to be employed.

Our parallel scheme and our data distribution are based on the realization that the Bethe Salpeter equation is the most time-consuming part of our calculation. One can easily see that it decouples nicely with respect to the bosonic momentum-frequency index Q. This enables us to distribute the vertices across processors with respect to this third index and to solve the Bethe-Salpeter equation with a local matrix inversion. However, this storage scheme puts a limit on the size of the problem that we can address. For a node with 2 GBytes of memory, the maximum value of n_t that we can use if our variables are complex double precision is about 2500.

Unlike the Bethe-Salpeter equation, one can readily observe that the parquet equation does not decouple in terms of the third index. Solving this equation requires a rearrangement of the matrix elements across processors and this is the communication bottleneck in the algorithm. The rearrangement is necessary to obtain the form of the vertex ladder Φ or Ψ that is required in the parquet equation. For instance, in the d channel, we need $\Phi(P-P')_{P,P+Q}$. This form of the vertex ladder is obtained by employing the three-step process described in the following equations:

$$\Phi(Q)_{P,P'} \Rightarrow \Phi(Q)_{P,P-P'}, \quad (13)$$

$$\Phi(Q)_{P,P-P'} \Rightarrow \Phi(P-P')_{P,Q}, \quad (14)$$

$$\Phi(P-P')_{P,Q} \Rightarrow \Phi(P-P')_{P,P+Q}. \tag{15}$$

The first step in this transformation only moves data locally in memory. This does not require much time. The second step is actually just a 2D matrix transpose but with matrix elements spreading on many nodes. This is where communication across nodes is required. It is achieved by using the standard message passing interface (MPI) collective directives [13]. The final step is also local and can equally be done very fast.

IV. RESULTS

In the following section, we will show the PA results for a 4×4 Hubbard cluster at half-filling. The calculations are done for $U=2t$ and different temperatures. The calculations are performed for a finite number of Matsubara frequencies [14]. However, for the observables we calculated, such as the local moment and magnetic susceptibility in Figs. 4 and 5, we performed an extrapolation to an infinite number of frequencies so that the cutoff error in frequency is minimized. To see how good PA works for the lattice model, we use the DQMC result as the benchmark. In the DQMC calculation, $\Delta\tau=1/12$ is used and the combined statistical and systematic errors are smaller than the symbols used. To further compare PA to other approximations, FLEX and self-consistent second-order results are also included.

A. Single-particle Green's function $G(\tau)$

First, one can get a rough idea of how PA improves the accuracy of physical observables by comparing the single-particle Green's function from different levels of approximation. Shown in Fig. 3 are $G_{\mathbf{k}}(\tau)$ with $\mathbf{k}=(\pi,0)$ and $\mathbf{k}=(0,0)$ calculated from the self-consistent second-order approximation, FLEX, PA, and DQMC. The parquet result is significantly closer to the DQMC result than the second-order approximation and FLEX results as can readily seen from the figure. This confirms the intuition that one would get better results if the approximation is made on the vertex which is most irreducible.

B. Unscreened local moment

Next we present results for the local magnetic moment defined as

$$\langle\mu\rangle \equiv \langle(n_\uparrow - n_\downarrow)^2\rangle, \tag{16}$$

$$= \langle n\rangle - 2\langle n_\uparrow n_\downarrow\rangle, \tag{17}$$

where $\hat{n}_\sigma$ denotes the number operator for electrons of spin σ. In the context of a conserving approximation, it can be re-expressed in terms of the self-energy and the single-particle Green's function as

$$\langle\mu\rangle = \langle n\rangle - \frac{2T}{U}\mathrm{Tr}(\Sigma G), \tag{18}$$

where the trace sums over both the momentum and the frequency degrees of freedom.

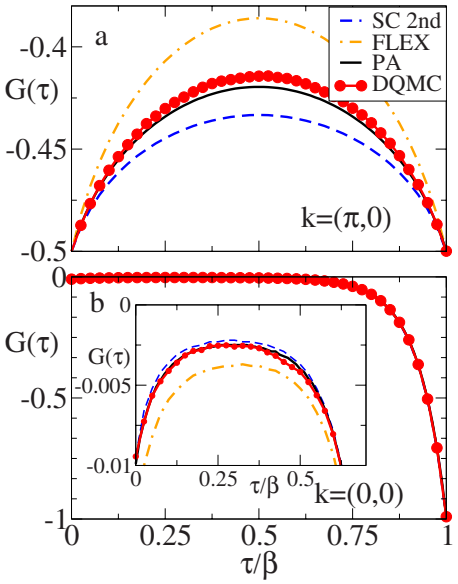

FIG. 3. (Color online) Single-particle Green's function $G(\tau)$ for two different momenta a), $\mathbf{k}=(\pi,0)$, b), $\mathbf{k}=(0,0)$, extracted from the three diagrammatic approaches and the DQMC. For this temperature ($T=0.3t$), the PA result (solid line) looks very close to the DQMC one (symbol solid line) as compared to SC second-order (dashed line) or FLEX (dash-dotted line). In the inset of (b) is an enlarged view of the figure.

The results are shown in Fig. 4. Among the three diagrammatic approaches, the PA result comes closest to the DQMC one. If we look more carefully at the DQMC curve, we can find the existence of two humps. The hump at $T_1 \simeq U/2$, which is well reproduced by the PA, designates the energy scale for the charge fluctuation, and is directly related to the suppression of charge double occupancy. The other hump beginning at $T_2 \ll t$ is related to the virtual exchange interaction, J, between nearby spins. It is believed to be related to the synergism between the development of the long-range antiferromagnetic correlation and enhancement of the local moment. As a result, a pseudogap is opened which increases the entropy of the system [15,16]. The magnitude of T_2 can be estimated by noticing $J=4t^2/U$ for the strong coupling limit and $t\exp(-2\pi t/U)$ in the weak coupling limit [15,17]. Therefore it basically interpolates between these two limits

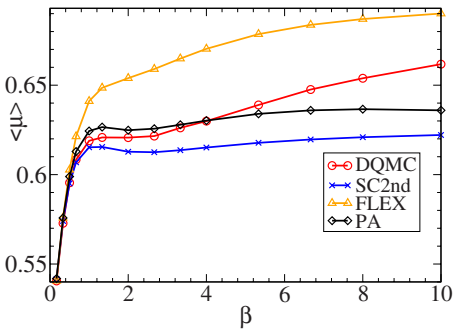

FIG. 4. (Color online) The inverse temperature dependence of local moment. Among the three diagrammatic approaches, the PA result comes closest to the DQMC one.

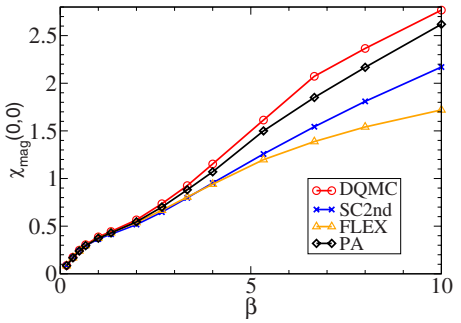

FIG. 5. (Color online) Uniform susceptibility calculated for different methods as a function of inverse temperature. While at the high temperature region, all the diagrammatic method results come close to the DQMC result, the PA shows its advantage clearly in the low temperature region.

for that $U=2t$ is in the intermediate coupling regime. This hump is not well captured by PA. The increasing importance of envelop-shape diagram contribution [3,5] not included in PA is responsible for this deviation in the low temperature region.

C. Uniform susceptibility

Finally, we look at the uniform magnetic susceptibility which is defined as

$$\chi_{mag}(0,0) = \int_0^\beta d\tau \langle \hat{T}_\tau S_z(\tau) S_z(0) \rangle \tag{19}$$

$$= \frac{1}{T} \langle S_z^2 \rangle \tag{20}$$

with magnetic moment defined as

$$\hat{S}_z(\tau) = \frac{1}{N} \sum_r [n_{r,\uparrow}(\tau) - n_{r,\downarrow}(\tau)]. \tag{21}$$

The χ_{mag} from different approaches are presented in Fig. 5. The uniform magnetic susceptibility calculated from DQMC follows a nearly linear dependence on β. This mimics closely the Curie-Weiss law of weakly interacting moments and implies that the dominant effect in the system is the short range magnetic fluctuation. This is consistent with the β dependence of the local moment presented in Fig. 4. As the temperature still dominates over the spin energy scale of the system, it suppresses the long-range fluctuation.

From this figure, the improvement of PA over the other two approximations is also easy to see. Similar to the local moment, the difference between results from PA and DQMC at the low temperature region can be explained by the omission of envelop-shape diagrams in PA.

V. SUMMARY AND OUTLOOK

We have presented the parquet formalism, PA method and in particular the implementation we use to solve large-sized problem. The preliminary application of PA on the 4×4 Hubbard cluster shows that it can yield better results than the self-consistent second-order or FLEX calculations. This is the first step in our work, next we are going to use the parquet formalism in the so-called multiscale many-body (MSMB) approach [18]. Within MSMB, correlations at different length scales are treated with different methods. The short length scales are treated explicitly with QMC methods, intermediate length scales treated diagrammatically using fully irreducible vertices obtained from QMC and long length scales treated at the mean field level. Note that in this approach the fully irreducible vertex is approximated by a QMC calculation on a small cluster, while in PA it is approximated by the bare interaction. Therefor this approach should provide superior results to the PA. Another advantage is that it can also avoid the exponential increase of the computational cost as the system size increases, and thus can take full advantage of the most up-to-date computer resources available. We will combine it with the local density approximation (LDA) to gain some predictive power from the first principle electronic structure calculation.

ACKNOWLEDGMENTS

We would like to acknowledge the very useful discussion with Gene Bickers and John Deisz. S.Y. also acknowledges the hospitality and support of the Institute for Theoretical Physics at the University of Göttingen, where part of this work has been performed. This work is supported by DOE SciDAC Project No. DE-FC02-06ER25792 which supports the development of Multi-Scale Many Body formalism and codes [18] and the DAAD through the PPP exchange program (T.P.). S.Y., H.F., K.T., and M.J. are also supported by the NSF PIRE Project No. OISE-0730290. This research used resources of the National Center for Computational Sciences at Oak Ridge National Laboratory, which is supported by the Office of Science of the U.S. Department of Energy under Contract No. DE-AC05-00OR22725.

[1] G. Baym and L. P. Kadanoff, Phys. Rev. **124**, 287 (1961).
[2] G. Baym, Phys. Rev. **127**, 1391 (1962).
[3] N. E. Bickers and S. R. White, Phys. Rev. B **43**, 8044 (1991).
[4] N. E. Bickers and D. J. Scalapino, Ann. Phys. **193**, 206 (1989).
[5] S. Allen, A.-M. S. Tremblay, and Y. M. Vilk, in *Theoretical Methods for Strongly Correlated Electrons*, edited by D. Senechal, A. Tremblay, and C. Bourbonnais (Springer-Verlag, New York, 2004), p. 341.
[6] C. de Dominicis and P. C. Martin, J. Math. Phys. **5**, 14 (1964).
[7] C. X. Chen and N. E. Bickers, Solid State Commun. **82**, 311 (1992).
[8] D. W. Hess, J. J. Deisz, and J. W. Serene, Philos. Mag. **74**, 457 (1996).

[9] N. E. Bickers, in *Theoretical Methods for Strongly Correlated Electrons*, edited by D. Senechal, A. Tremblay, and C. Bourbonnais (Springer-Verlag, New York, 2004), p. 237.
[10] G. L. G. Sleijpen and D. R. Fokkema, Electron. Trans. Numer. Anal. **1**, 11 (1993).
[11] Y. Saad and M. H. Schultz, SIAM (Soc. Ind. Appl. Math.) J. Sci. Stat. Comput. **7**, 856 (1986).
[12] D. D. Johnson, Phys. Rev. B **38**, 12807 (1988).
[13] For a detailed description of MPI, we refer to http://www.mcs.anl.gov/research/projects/mpi/.
[14] We use the periodic boundary condtions in the frequency space for the ease of implementation. And we have checked that different boundary conditions converge to the same result as n_f increases.
[15] T. Paiva, R. T. Scalettar, C. Huscroft, and A. K. McMahan, Phys. Rev. B **63**, 125116 (2001).
[16] S. Moukouri and M. Jarrell, Phys. Rev. Lett. **87**, 167010 (2001).
[17] J. E. Hirsch, Phys. Rev. B **31**, 4403 (1985).
[18] C. Slezak, M. Jarrell, Th. Maier, and J. Deisz, e-print arXiv:cond-mat/0603421; M. Jarrell, K. Tomko, Th. Maier, E. D'Azevedo, R. T. Scalettar, Z. Bai, and S. Savrasov, J. Phys.: Conf. Ser. **78**, 012031 (2007).